DCC Receptors Drive Prefrontal Cortex Maturation by Determining Dopamine Axon Targeting in Adolescence

Supplemental Information

Supplementary Methods and Materials

Animals

All experiments and procedures were performed in accordance with the guidelines of the Canadian Council of Animal Care and the McGill University/Douglas Mental Health University Institute Animal Care Committee. Mice were bred in the Douglas Mental Health University Institute Neurophenotyping Center, maintained on a 12-h light–dark cycle (light on at 0800 h) and given ad libitum access to food and water unless noted. Pups were weaned at postnatal day (PND) 21±1 and housed with same-sex littermates. Only male mice were used in experiments.

Dcc conditional mice. We have induced *Dcc* haploinsufficiency exclusively in dopamine neurons by crossing mice with loxP-insertions flanking exon 23 of one *Dcc* allele ($Dcc^{lox/+}$) (1) with a line in which iCre expression is regulated by the dopamine transporter (DAT^{Cre}; BAC-*DATiCre* mice) (2). These $Dcc^{lox/+}DAT^{Cre}$ mice survive to adulthood and do not exhibit any overt phenotypic differences from control *Dcc*-floxed littermates. Floxed, cre-negative littermates ($Dcc^{lox/+}$) are indistinguishable from wild-type mice, and were utilized as experimental controls. To determine axonal architecture, DAT^{Cre} mice lacking any floxed alleles were utilized as experimental controls as these mice express Cre recombinase under the DAT promoter and are otherwise indistinguishable from wild-type mice. Adolescent $Dcc^{lox/+}$ mice were utilized in the viral tracing experiments, and their wild-type littermates ($Dcc^{+/+}$) were used as controls.

Different cohorts of control and experimental mice were used for each experiment. Each experiment had cohorts from a minimum of 5 litters.

Axon-initiated recombination in adolescence

Experimental strategy. To track the growth of dopamine axons during adolescence, we have adapted an axon-initiated viral transduction technique (3) for specific labeling of midbrain neurons that terminate in the ventral striatum at the start of adolescence. At PND21, we injected a retrogradely transported virus expressing Cre recombinase (CAV-Cre, BioCampus Montpellier, Titer: $3.8x10^{12}$pp/mL) (4; 5) unilaterally at the level of the NAcc. We simultaneously injected a Cre-dependent enhanced yellow fluorescent protein (eYFP) virus (pAAV-Ef1a-DIO-EYFP-WPRE-pA, UNC Vector Core, Titer: $6x10^{12}$pp/mL) into the ipsilateral VTA. CAV-Cre is preferentially taken up by axon terminals (4; 5). The CAV vector binds to the Coxsackievirus and adenovirus receptor (CAR) and, together, they are endocytosed and transported retrogradely along axons. This CAR-mediated internalization limits CAV vector uptake to axon terminals (4), thus this recombination strategy limits eYFP labeling to VTA neurons with axons that terminate in the NAcc at PND21 (Figure 1A).

Stereotaxic surgery. Early adolescent (PND21±1) *Dcc*$^{lox/+}$ or wild-type mice were anesthetized with isoflurane. Simultaneous unilateral stereotaxic infusions of DIO-eYFP into the VTA and CAV-Cre into the NAcc were performed using Hamilton syringe needles. *VTA coordinates*: -2.56 mm (anterior/posterior), +0.9 mm (lateral), and -4.1 mm (dorsal/ventral) relative to Bregma, at a 10° angle. *NAcc coordinates*: +2.6 mm (anterior/posterior), +1.5 mm (lateral), and -3.75 mm (dorsal/ventral) relative to Bregma, at a 30° angle. A total of 0.5 µl of purified virus was delivered on each side over an 8-min period followed by a pause of 6 min. VTA coordinates in PND21 mice were as previously (2), and NAcc placements were adapted from adult coordinates and first verified by dye injection in a separate set of wild-type PND21

animals. Adult (PND75±15) wild-type mice underwent the same injection procedure using the following coordinates: *VTA*: -3.2 mm (anterior/posterior), +1.0 mm (lateral), and -4.6 mm (dorsal/ventral) relative to Bregma, at a 10° angle. *NAcc*: +1.8 mm (anterior/posterior), +3.0 mm (lateral), and -4.8 mm (dorsal/ventral) relative to Bregma, at a 30° angle (2; 6).

Immunofluorescence. Mice that received viral injections at PND21 were transcardially perfused at PND60 with 4% paraformaldehyde, and their brains prepared for immunofluorescence as previously (7; 8). Mice that received viral injections in adulthood were processed for immunofluorescence after a 4-5 week incubation period to allow complete eYFP labeling. Briefly, 35μm sections were incubated with a polyclonal anti-GFP raised in chicken (1:1000, antibody #1020, Aves labs) and a polyclonal rabbit anti-TH antibody (1:1000, AB152, Millipore Bioscience Research Reagents). Immunostaining was visualized with Alexa Fluor 488- and Alexa Fluor 555-conjugated secondary antibodies raised in goat (1:500; Invitrogen) and slides were coverslipped with DAPI.

Stereology. We performed stereological quantification of (a) the span and density of TH-positive innervation, (b) the number of TH-positive, eYFP-positive varicosities, and (c) the number of TH-negative, eYFP-positive varicosities in the cingulate (Cg1) and prelimbic (PrL) subregions of the pregenual mPFC and the NAcc (2; 7; 8). We also quantified (a) the number of TH-positive neurons, (b) the number of eYFP-labeled TH positive neurons, and (c) the number of TH-negative, eYFP-positive neurons in midbrain regions where we observed recombination, including the ventral tegmental area (VTA) and substantia nigra pars compacta (SNc).

To assess the span of TH-positive fiber innervation (total volume in cubic micrometers) we used the Cavalieri method in Stereoinvestigator® (MicroBrightField) (2; 7). To determine the number of TH-

positive, eYFP-positive, and co-labeled varicosities we used the optical fractionator probe of the Stereoinvestigator software. As in all our previous neuroanatomical studies, we obtained counts only from the right hemisphere because of the lateralization of dopamine systems. The coefficient of error (CE) for stereological quantification of TH-positive varicosities was below 0.06 for all regions of interest in all sampled brains. The CE for eYFP/TH-positive co-labeled varicosities was below 0.16 for all regions of interest in mice that received virus injections during adolescence. Due to the low number of eYFP/TH-positive co-labeled varicosities in mice that received dual viral injections during adulthood, the CE was often high (>0.2), indicating that these rare varicosities are not reliably stereologically quantifiable. Counts were performed blind.

mPFC analysis: The cingulate (Cg1) and prelimbic (PrL) subregions of the mPFC were delineated according to plates spanning 14 – 18 of the mouse brain atlas (9). Contours of the dense TH-positive innervation of the Cg1 and PrL subregions were traced at 5X magnification using a Leica DM400B microscope. An unbiased counting frame (50 x 50 μm) was superimposed on each contour and counts were made at regular predetermined intervals (x= 175 μm, y= 175 μm) from a random start point. TH positive and eYFP positive varicosities were counted at 100X magnification on 5 sections contained within the rostrocaudal borders of our region of interest (Plates 14-18; 1:4 series, Figure S1G). A guard zone of 4 μm was used and the optical disector height was set to 10 μm.

NAcc analysis: An unbiased counting frame (10 x 10 μm) was superimposed on the contour of the NAcc and counts were made at regular predetermined intervals (x= 400 μm, y= 400 μm) from a random start point. Counting was performed at 100X magnification on four of the eight sections contained within the rostrocaudal borders of our region of interest (Plates 15–18, 1:4 series. A guard zone of 4μm was used and the optical disector height was set to 5μm.

Midbrain analysis: The total number of TH-positive and eYFP/TH-positive co-labeled dopamine neurons in the VTA and SNc was assessed using the optical fractionator probe of Stereoinvestigator. The counting scheme used a 60 × 60 μm counting frame (x =150 μm, y = 150 μm intervals) with a random start point. Counting was performed at 40X magnification in a 1:4 series. A 3 μm guard zone and a probe depth of 10 μm were used. Stereological counts of eYFP and TH co-labeled neuron populations were expressed as proportions.

Data analysis. Two-way mixed-design ANOVAs with genotype as a between-subjects factor and subregion as a within-subjects factor were used to analyze the number of eYFP/TH-positive co-labeled varicosities in Cg1 and PrL subregions of the mPFC. The effects of *Dcc* on the development of dopamine connectivity in the mPFC vary along the dorso-ventral axis (2; 7); thus here, as in our previous studies, we include subregion as one of the main factors in the analysis. Two-way ANOVAs with region and treatment as between-subjects variables were used to analyze the proportion of dopamine neurons labeled with eYFP, and the proportion of eYFP-positive neurons that were dopaminergic in the VTA and SNc for each group. Correlations were calculated using the Pearson correlation coefficient with one-tailed analysis.

Quantitative analysis of dopamine axon architecture

Stereotaxic surgery. Adult (PND60) *Dcc*$^{lox/+}$*DAT*^{Cre} or DAT^{Cre} mice were anesthetized with isoflurane. Bilateral VTA stereotaxic infusions of the Cre-dependent fluorophore virus DIO-eYFP (AAV-EF1a-DIO-EYFP; UNC Vector Core) were performed using Hamilton syringe needles at the following coordinates: -3.2 mm (anterior/posterior), +1.0 mm (lateral), and -4.6 mm (dorsal/ventral) relative to Bregma, and at

a 10° angle. A total of 0.5 µl of purified virus was delivered on each side over an 8-min period followed by a pause of 6 min.

Immunofluorescence. 4-5 weeks after virus injections, mice were transcardially perfused with 4% paraformaldehyde and their brains prepared for immunofluorescence. Sections of brain 35µm thick were incubated with a polyclonal anti-GFP raised in chicken (1:500, antibody #1020, Aves Labs) and immunostaining was visualized with Alexa Fluor 488-conjugated secondary antibodies raised in goat. Sections were mounted on slides and coverslipped with DAPI.

Axon tracing. Regions of interest were delineated according to the mouse brain atlas (9) at 5x magnification with a Leica DM4000B microscope. Only eYFP-positive axons with intact arbors, defined as having all of the tips of their terminal branches within the section, were included in the analyses. Individual axon arbors were identified at 20x magnification. Neurolucida software (MicroBrightField) was used to trace the terminal arbors of selected axons at high magnification (40x), and to quantify axon arbor length, complexity, and varicosity density of each axon.

Data analysis. To quantify the complexity of individual dopamine axons, we adapted the Axonal Complexity Index (ACI) from developmental studies using Xenopus tadpoles (10). Two-way mixed-design ANOVAs with genotype as a between-subjects factor and subregion as a within-subjects factor were used to analyze axon arbor length, complexity, and varicosity density.

Western blot analysis of Netrin-1 protein in dopamine terminal regions

Whole brains from PND75±15 male $Dcc^{lox/+}$ or $Dcc^{lox/+}DAT^{Cre}$ mice were flash frozen in 2-methylbutane. Bilateral punches of the prefrontal cortex, dorsal striatum and nucleus accumbens were processed for

western blot as before (11; 12). Briefly, protein samples (15 μg) were separated on a 10% SDS-PAGE and transferred to a nitrocellulose membrane which was incubated overnight at 4°C with antibodies against Netrin-1 (1:750, Novus Biologicals, Littleton, CO, USA) and β-actin (1:15000, Sigma-Aldrich, Oakville, ON, Canada) for loading control. Protein bands were detected by chemiluminescence (Perkin Elmer, Waltham, MA, USA) and analysed using Kodak Imaging system software (2000, New Haven, CT, USA).

Data analysis: Samples were grouped by genotype and their chemiluminescence was compared using two-tailed Students t-tests for each region of interest.

Quantification of pyramidal neuron morphology

Golgi–Cox staining. Mice were anesthetized with sodium pentobarbital (>75 mg/kg; i.p.) and perfused transcardially with 0.9% saline. The brains were processed for Golgi-Cox staining as previously (7; 13) .

Anatomical analysis. Basilar dendritic arbors and spines of layer V mPFC pyramidal neurons were analyzed to quantify the total arbor length, number of branches, and spine density of each cell. Neurons from the cingulate (Cg1) and prelimbic (PrL) subregions of the pregenual mPFC were analyzed. A Leica model DM400 microscope equipped with a Ludl XYZ motorized stage was used to identify cells, trace dendritic arbors, and quantify dendritic spines. Relevant regions were first identified at low magnification (5X objective). Cells that were chosen for tracing and analysis were required to have intact branches, well impregnated staining, and not obscured by blood vessels, astrocytes, or heavy clusters of dendrites from other cells. Neurolucida software (MicroBrightField) was used to trace the dendritic arbors of selected cells and to quantify dendritic arbor length, dendrite number, and the spine density on selected dendrite segments (100X objective). For both dendritic arbor and spine density analysis, the same neurons were sampled. One dendritic segment (third-order tip or greater) was analyzed per

neuron. Spines were always counted from the last branch point to the terminal tip of the dendrite. No attempt was made to correct for the fact that some spines are obscured from view, so the measure of spine density necessarily underestimates total spine density. Anatomical analysis was conducted blind to treatment condition. A minimum of four cells were analyzed per brain, and averaged across each subject.

Data analysis. To quantify the complexity of individual dopamine axons, we used the Dendritic Complexity Index (DCI) (14). Neurons from individual mice were averaged within each subregion and then grouped by genotype to analyze dendritic arbor length, branch number, DCI, and spine density by two-way mixed-design ANOVAs with genotype as a between-subjects factor and subregion as a within-subjects factor.

Behavior

Go/No-Go. During behavioral testing, mice were food restricted to 1.5 g food per day for the duration of the task in order to maintain a body weight that was 85% of the initial free feeding weight. We used a modified mouse Go/No-Go Task which was optimized for our operant equipment (15; 16). Sessions took place in operant behavioral boxes (Med Associates, Inc., St Albans, VT, USA) that are equipped with a house light, an adjustable Sonalert tone generator, two illuminated nose poke holes (Right and Left), a clicker, and a pellet dispenser. The boxes were situated in sound attenuating ventilated cubicles (Med Associates, Inc.). We used chocolate-flavored dustless precision pellets (BioServ, Inc., Flemington, NJ, USA) as our operant reinforcer. The experimental procedure consisted of three stages: Conditioned Reinforcement Training, Reaction Time Training, and the Go/No-Go Task. Animals were subject to one training or testing session per day.

Conditioned reinforcement training. At the start of each Conditioned Reinforcement session, the house light comes on and remains on throughout the 20 minute session. Each trial consists of the presentation of an illuminated nose poke hole for 9 seconds. If the mouse does not respond by nose-poking in the illuminated hole, the cue light is extinguished for a 10 second inter-trial interval (ITI) before the next trial/cue presentation. If the mouse responds to the cue light by nose-poking in the illuminated hole, a chocolate food pellet is dispensed and the trial is counted as a "reward" trial. The location of the active (cued) nose poke hole (either Left or Right) was counterbalanced within groups, and stayed consistent for each individual mouse for the duration of the session and throughout each stage of the experiment. Responses to the active nose poke hole when the cue light is off, as well as responses to the non-active nose poke hole (where the cue light was never illuminated), do not result in a reward but were recorded and analyzed. Mice advanced to the next stage of training once they achieve a criterion of over 70% responses to cued trials. Mice received one 20 minute Conditioned Reinforcement training session per day.

Reaction time training. Once mice stably respond to the cued nose poke hole to receive the reinforcer, they are trained to 1) respond only following the illumination of the cue light, and 2) to respond within 3 seconds of the cue illumination to receive the reinforcer. To train mice to respond only when the cue light is present, the structure of the session was changed to incorporate a pretrial period prior to each trial. In this pretrial period, the house light was illuminated for a variable amount of time (3, 6, or 9 seconds, distributed randomly) *without* the cue light. If the mouse nose poked during this pretrial period, the house light was extinguished and a 10 second ITI was initiated. This was recorded as a 'Premature Response'. If the mouse did not respond during the pretrial period, the cue light was then illuminated for 3 seconds. A response during this 3 second trial period resulted in the delivery of a reward pellet; if the mouse failed to respond within this window, the cue and house lights were

extinguished and a 10 second ITI began. In order to advance to the Go/No-Go Task, mice had to end less than 25% of the pretrial periods with a premature response. Mice received one 30 minute reaction time training session per day.

Go/No-Go task. Following successful completion of both training stages, mice underwent 10 sessions of the Go/No-Go Task. This task required the mice to respond to a lighted 'Go' cue, identical to the cue used in the training sessions, or inhibit their response to this cue when presented in tandem with an auditory 'No-Go' cue. In the 'Go' trials, mice had to respond to the illuminated nose poke hole in the 3-second timeframe during which the cue light was on in order to receive a reward. This was counted as a 'Hit' in our analysis. In the 'No-Go' trials, an 80 dB tone was paired with the 3-second cue light to signal that the mouse should withhold from responding. If mice responded during the 3- second 'No-Go' trial, an ITI was initiated and no reward was dispensed. This was counted as a 'Commission Error' in our analysis. However, if mice withheld from responding for the 3 second duration of the tone/light 'No-Go' cue, a reward was dispensed. As in the Reaction Time training, a randomized, variable pretrial period of 3-9 seconds preceded each trial and the number of premature responses was recorded. Within each session, the number of 'Go' and 'No-Go' trials were given in an approximately 1:1 ratio and presented in a randomized order. Each session lasted 30 minutes and consisted of approximately 30-50 'Go' and 30-50 'No-Go' trials.

Attentional set-shifting task (ASST): The ASST was performed as previously (2). Briefly, mice were food restricted to 85% of free feeding body weight during the ASST and trained to dig for a food reward (Froot Loops) based on two dimensions of stimuli. The ASST phases included 1) a simple discrimination (SD), in which mice had to discriminate along one stimulus dimension (i.e. between two digging mediums); 2) a compound discrimination (CD), in which a new stimulus dimension was introduced (i.e.

odor) but the same previously trained discrimination was required; 3) an intra-dimensional shift (ID), in which new combinations of odors and digging mediums were presented, but the rewarded cue remained along the same stimulus dimension (i.e.. digging medium); 4) an extra-dimensional shift (ED), in which new stimuli were introduced, but now the rewarded stimulus dimension was changed (i.e. between two odors). Each stage was completed when the mice were able to reach a learning criterion of six consecutive correct choices (2; 17).

Morris water maze: The Morris water maze was a metallic, circular pool (1.44 m inner diameter x 23cm depth), located in an illuminated, sound-attenuated room (18). The pool was filled out with warm water 15cm below the rim, and temperature was maintained at ±23ºC. Water was made opaque with a non-toxic white tempera that was stirred daily to make an even distribution. The maze was divided with two imaginary lines that crossed on the center of the pool in a perpendicular manner to demarcate four equal size quadrants, labeled as A, B, C, and D, A being opposite to C, and B opposite to D. The end of each line designated the North (N), West (W), East (E), and South (S). A circular white platform (12cm diameter) was used as escape platform, and was always hidden 1.5cm below the water surface. The platform was easily removable and located in the middle of one quadrant; either at north-west (NW), north-east (NE), south-west (SW), or south-east (SE) coordinates. There were a total of eight starting positions marked in the outer faces of the pool: N, W, E, S, NW, NE, SW, and SE. Several room cues and extra-maze cues surrounded the pool, and an over-head camera was located on the ceiling for behavioral recording. Animals' behavior was registered with the Tracking System HVS Image (Buckingham, UK), for offline analysis. The latency to find the platform, the swimming speed and the total path length were registered during the training, and results were estimated in block of trials per session (average of the four trials). The percentage of time spent in each quadrant and the number of

entries into platform area were recorded during the test, as well as the swimming speed and the total path length.

Spatial task: The spatial task consisted of two phases: the training and the test. For the training, mice received five daily sessions of four trials with the hidden platform and the presence of extra-maze cues. The position of the platform was selected randomly, and located in the middle of one of the quadrants (i.e. NW), at 20 cm from the pool wall. The starting positions were chosen pseudo-randomly, depending on the distance from the platform, thus, the more distal positions were used to avoid response learning. These positions were different from session to session but were identical within a session for all the animals. Each mouse was released into the water at the edge of the pool facing the walls and allowed to swim until it found the platform or until 60 sec had elapsed. If the mouse did not find the platform within the allotted time, it was gently directed to it by the experimenter. Mice were left on the platform for 30 sec; thereafter, they were dried out with a towel, and returned to the holding cage for an inter-trial interval of approximately 20 minutes. The spatial test day was twenty-four hours after the last training trial to avoid the use of recent memory acquired during the training (18), and consisted of placing the mice in the pool to swim for 60 sec in the absence of the platform.

Elevated plus maze: Mice were assessed in an Elevated Plus Maze (EPM) for anxiety-like behaviors. The maze consisted of two facing open arms and two facing enclosed arms that extend from a central platform elevated 50 cm from the floor. Mice were placed in the center platform of the maze facing one of the open arms and left to explore the arms during five minutes. The number of entries and total time spent in the open *versus* closed arms of the maze were recorded with an overhead video camera for offline analysis using the software TopScan™ 2.0 (Clever Sys., Reston, Virginia, USA).

Open field: Locomotor activity in a novel open field over 15 minutes was recorded with an overhead video camera for offline analysis using the software TopScan™ 2.0 (Clever Sys., Reston, Virginia, USA). Locomotion was measured as distance travelled (cm).

Behavioral data analysis:

Go/No-Go task. For Conditioned reinforcement training and Reaction Time training, mice were grouped by genotype and the number of days to reach criterion was analyzed between genotypes with a two-tailed Students t-test. For the Go/No-Go task, mice were grouped by genotype and the number of Commission errors and Hits (correct responses to the 'Go' cue) were analyzed over 10 testing days using a two-way mixed design ANOVA with genotype as a between-subjects factor and day as a within-subjects factor.

ASST. Number of trials to criterion and number of errors made within each of the 4 aspects of the ASST task (SD, CD, ID, ED) were recorded manually. Mice were grouped by genotype and ASST performance was analyzed using a two-way mixed design ANOVA with genotype as a between-subjects factor and task (e.g. ID or ED) as a within-subjects factor, followed by post-hoc Bonferroni tests.

Morris Water Maze. Mice were grouped by genotype and latency to reach the platform on each training day was analyzed using a two-way mixed design ANOVA with genotype as a between-subjects factor and training day as a within-subjects factor. The percentage of time spent in each quadrant during the probe trial was analyzed using a two-way mixed design ANOVA with genotype as a between-subjects factor and quadrant as a within-subjects factor.

EPM and open field. For the EPM, mice were grouped by genotype and the percentage of entries into the open arms and the percentage of time spent in the open arms of the maze were compared using two-tailed Students t-tests. For novel open field, mice were grouped by genotype and locomotor activity (distance traveled in cm) and the percentage of time spent in the center of the open field was compared using two-tailed Students t-tests. All statistical analyses were carried out using Prism software (GraphPad).

Supplementary Figures

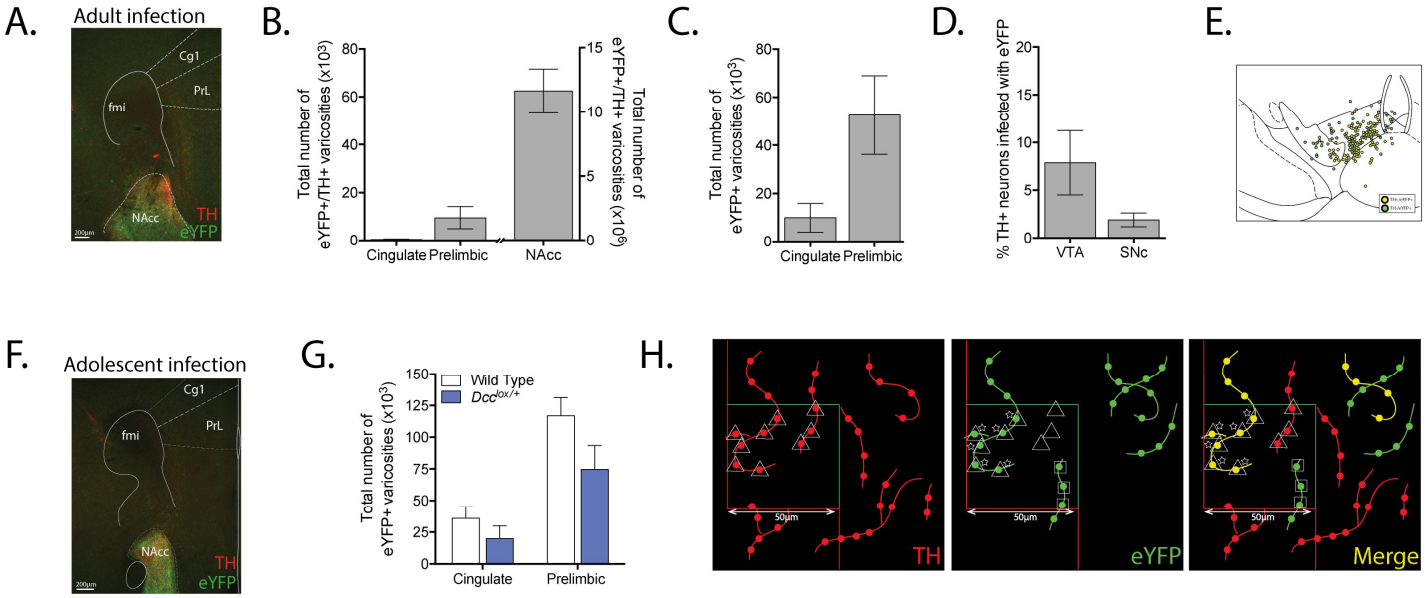

Figure S1: Stereological quantification of eYFP-positive dopamine axons.
(A) Low magnification image of a coronal section from a mouse that was injected with the tracing viruses in adulthood, stained for TH (red) and eYFP (green) with regions demarcated according to the Mouse Brain Atlas (9). Cg1 – cingulate subregion of the mPFC; PrL –Prelimbic subregion of the mPFC; NAcc – nucleus accumbens; fmi – forceps minor of the corpus callosum. (B) Stereological quantification reveals that although there are both TH-positive and eYFP-positive varicosities in the mPFC of mice that received virus injections in adulthood, varicosities co-labeled with TH and eYFP are rare and stereologically unreliable (Coefficient of error > 0.2, n = 3). In contrast, the NAcc receives dense eYFP-positive dopamine innervation. (C) eYFP-positive, non-dopaminergic varicosities are present in the mPFC of mice that received virus injections in adulthood. (D) Percentage of eYFP-positive dopamine neurons in the VTA and SNc of mice that received injections of viral tracers in adulthood is comparable to those that received tracers in adolescence. (E) Distribution map of stereological markers for TH-positive/eYFP-positive neurons in the VTA and SNc of mice that received viral injections in adulthood. (F) Low magnification image of a coronal section from a mouse injected with the tracing viruses in adolescence, stained for TH (red) and eYFP (green) with regions demarcated according to the Mouse Brain Atlas (9). (G) eYFP-positive, non-dopaminergic varicosities are also present in the mPFC of wild type and *Dcc*$^{lox/+}$ mice that received virus injections in adolescence. (Two-way mixed-design ANOVA, no effect of genotype, $F_{(1, 8)} = 2.61$, $p = 0.14$; main effect of subregion, $F_{(1, 8)} = 100.2$, $p < 0.0001$; no genotype x subregion interaction, $F_{(1, 8)} = 3.757$, $p = 0.09$. n = 5 per group). (H) Diagram of stereological quantification of TH-positive/eYFP-positive varicosities. A 50µm x 50µm counting frame was overlaid on the live microscope image in Stereoinvestigator. TH-positive/eYFP-positive varicosities were counted if they 1) were contained within the counting frame or touching the green, but not the red, outer boundaries of the counting frame, and 2) were clearly labeled for both TH and eYFP. This was achieved

by placing an open maker (*triangle*) over each TH-positive varicosity while working within the red channel. Next, the channel was switched to green while the slide remained in the same area and markers were placed over eYFP-positive varicosities that were already marked for TH (*stars*) and those that were not co-labeled for TH (*squares*).

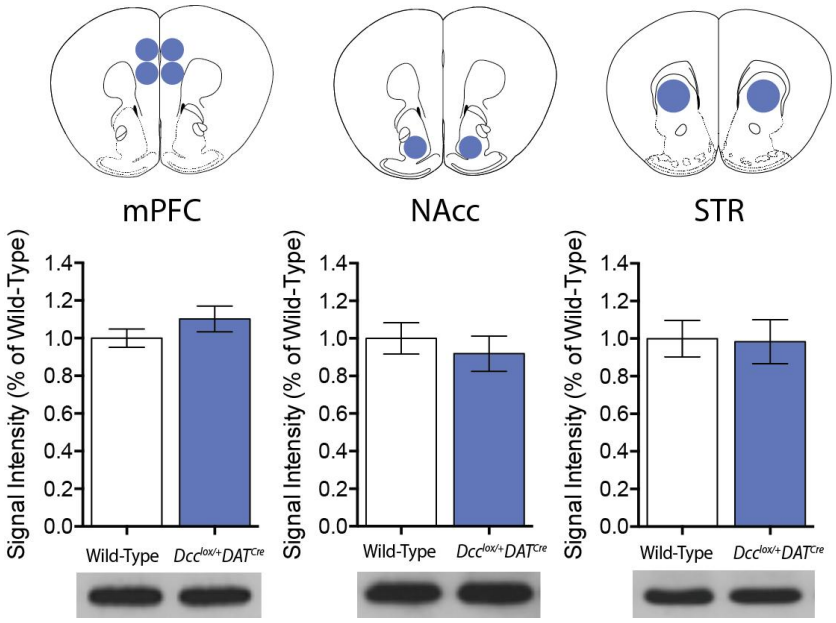

Figure S2: *Dcc*$^{lox/+}$*DAT*^{Cre} mice have normal Netrin-1 protein expression in dopamine terminal regions. *Dcc* haploinsufficiency in dopamine neurons does not alter the expression of Netrin-1, the ligand for DCC, in corticostriatal dopamine terminal regions (mPFC: $t_{(13)} = 1.229$, $p = 0.12$; NAcc: $t_{(13)} = 0.6504$, $p = 0.52$; STR: $t_{(13)} = 0.1083$, $p = 0.91$. *Dcc*$^{lox/+}$*DAT*^{Cre} n = 7; Wild-type n = 8).

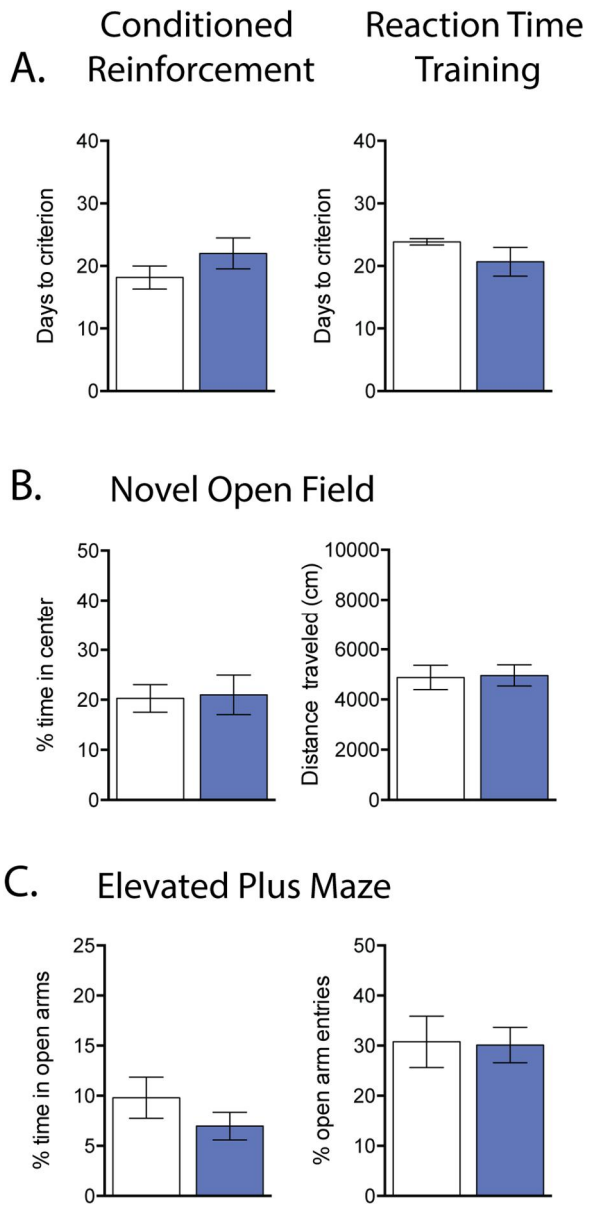

Figure S3: *Dcc*$^{lox/+}$*DAT*^{Cre} mice have improved behavioral flexibility without differences in PFC-independent behaviors.

(A) There were no differences in learning during the preliminary stages of the Go/No-Go task, where mice learned to nose poke to receive a reward only when a cue is present (*Conditioned Response, left panel*: $t_{(11)} = 2.72$, p =0.23. *Reaction Time Training, right panel*: $t_{(11)} = 1.449$, p =0.175. *Dcc*$^{lox/+}$*DAT*^{Cre} n = 6; Wild-type n = 7). (B) No differences were found between genotypes in the percentage of time on the open arms or percentage of entries into the open arms of the Elevated Plus Maze (*Percentage of time in open arms, left panel*: $t_{(11)} = 1.099$, p = 0.29; *Percentage of open arm entries*, *right panel*: $t_{(11)}$=0.1036, p = 0.91. *Dcc*$^{lox/+}$*DAT*^{Cre} n = 6; Wild-type n = 7). (C) *Dcc*$^{lox/+}$*DAT*^{Cre} mice were not different from wild-type littermates in locomotor activity or time in the center of a novel open field (*Distance traveled, left panel*: $t_{(11)} = 0.1240$, p = 0.90; *Percentage of time in center of open field, right panel*: $t_{(11)} = 0.1481$. p = 0.88. *Dcc*$^{lox/+}$*DAT*^{Cre} n = 6; Wild-type n = 7).

Supplementary References

1. Krimpenfort P, Song J-Y, Proost N, Zevenhoven J, Jonkers J, Berns A (2012): Deleted in colorectal carcinoma suppresses metastasis in p53-deficient mammary tumours. *Nature*. 482: 538–541.

2. Manitt C, Eng C, Pokinko M, Ryan RT, Torres-Berrío A, Lopez JP, *et al.* (2013): dcc orchestrates the development of the prefrontal cortex during adolescence and is altered in psychiatric patients. *Transl Psychiatry*. 3: e338.

3. Beier KT, Steinberg EE, DeLoach KE, Xie S, Miyamichi K, Schwarz L, *et al.* (2015): Circuit Architecture of VTA Dopamine Neurons Revealed by Systematic Input-Output Mapping. *Cell*. 162: 622–634.

4. Bru T, Salinas S, Kremer EJ (2010): An update on canine adenovirus type 2 and its vectors. *Viruses*. 2: 2134–2153.

5. Soudais C, Laplace-Builhe C, Kissa K, Kremer EJ (2001): Preferential transduction of neurons by canine adenovirus vectors and their efficient retrograde transport in vivo. *The FASEB Journal*. 15: 2283–2285.

6. Daubaras M, Dal Bo G, Flores C (2013): Target-dependent expression of the netrin-1 receptor, UNC5C, in projection neurons of the ventral tegmental area. *Neuroscience*. doi: 10.1016/j.neuroscience.2013.12.007.

7. Manitt C, Mimee A, Eng C, Pokinko M, Stroh T, Cooper HM, *et al.* (2011): The netrin receptor DCC is required in the pubertal organization of mesocortical dopamine circuitry. *J Neurosci*. 31: 8381–8394.

8. Reynolds LM, Makowski CS, Yogendran SV, Kiessling S, Cermakian N, Flores C (2015): Amphetamine in Adolescence Disrupts the Development of Medial Prefrontal Cortex Dopamine Connectivity in a dcc-Dependent Manner. *Neuropsychopharmacology*. 40: 1101–1112.

9. Paxinos G, Franklin KBJ (2008): *The Mouse Brain in Stereotaxic Coordinates*. Academic Press.

10. Marshak S, Nikolakopoulou AM, Dirks R, Martens GJ, Cohen-Cory S (2007): Cell-autonomous TrkB signaling in presynaptic retinal ganglion cells mediates axon arbor growth and synapse maturation during the establishment of retinotectal synaptic connectivity. *J Neurosci*. 27: 2444–2456.

11. Grant A, Hoops D, Labelle-Dumais C, Prévost M, Rajabi H, Kolb B, *et al.* (2007): Netrin-1 receptor-deficient mice show enhanced mesocortical dopamine transmission and blunted behavioural responses to amphetamine. *Eur J Neurosci*. 26: 3215–3228.

12. Manitt C, Labelle-Dumais C, Eng C, Grant A, Mimee A, Stroh T, Flores C (2010): Peri-pubertal emergence of UNC-5 homologue expression by dopamine neurons in rodents. *PLoS ONE*. 5: e11463.

13. Gibb R, Kolb B (1998): A method for vibratome sectioning of Golgi-Cox stained whole rat brain. *J Neurosci Methods*. 79: 1–4.

14. Lom B, Cohen-Cory S (1999): Brain-derived neurotrophic factor differentially regulates retinal ganglion cell dendritic and axonal arborization in vivo. *J Neurosci*. 19: 9928–9938.

15. Loos M, Staal J, Schoffelmeer ANM, Smit AB, Spijker S, Pattij T (2010): Inhibitory control and response latency differences between C57BL/6J and DBA/2J mice in a Go/No-Go and 5-choice serial reaction time task and strain-specific responsivity to amphetamine. *Behav Brain Res*. 214: 216–224.

16. Gubner NR, Wilhelm CJ, Phillips TJ, Mitchell SH (2010): Strain differences in behavioral inhibition in a Go/No-go task demonstrated using 15 inbred mouse strains. *Alcohol Clin Exp Res*. 34: 1353–1362.

17. Birrell JM, Brown VJ (2000): Medial frontal cortex mediates perceptual attentional set shifting in the rat. *J Neurosci*. 20: 4320–4324.

18. Vorhees CV, Williams MT (2006): Morris water maze: procedures for assessing spatial and related forms of learning and memory. *Nat Protoc*. 1: 848–858.